Tuning to Resonances With Iterative Time Reversal

Jerry Kim, *Student Member, IEEE*, Margaret Cheney, *Senior Member, IEEE*, and Eric Mokole, *Fellow, IEEE*

***Abstract*— This paper considers a distributed wave-based sensing system that probes a scene consisting of multiple interacting idealized targets. Each sensor is a collocated transmit–receive pair that is capable of transmitting arbitrary wideband waveforms. We address the problem of finding the space-time transmit waveform that provides the best target detection performance in the sense of maximizing the energy scattered back into the receivers. Our approach is based on earlier theoretical work that showed, for an idealized infinite half-space geometry, that the solution could be constructed by an iterative time-reversal (TR) process. In this paper, we give a more realistic example involving a two-sensor time-domain system. We show that for this system, the iterative TR process can be used to tune automatically to all the target resonances that are within the bandwidth of the interrogating radar system. We show that although obtaining eigenvalues (and hence resonances) of the scattering operator is in general unstable, using the iterative TR process to obtain the resonances is a stable process. Moreover, we show that these resonance frequencies are connected to the poles of the singularity expansion method.**

***Index Terms*— Detection theory, eigenvalues, inverse scattering, multiple input multiple output, multiple sensors, power method, singularity expansion method (SEM), time reversal (TR).**

I. Introduction

THIS paper addresses the problem of finding the space-time waveform that results in the most energy scattered back to sensors from a distant target. This problem is relevant, for example, in detecting a weakly scattering target at maximum possible range. We consider the case in which a small number of ideal discrete sensors both transmit and receive, so that the problem becomes one of determining the time-domain waveforms that should be transmitted by the different sensors so that those sensors receive the maximum scattered energy.

The problem of increasing the scattered energy received by the sensors has been previously studied by a number of authors. For a single sensor, [1] proposed an approach based on trying different frequencies in a random sequence. For multiple sensors, received signal energy can be increased by a process known as the time-reversal (TR) process [2], in which scattered signals are recorded at the receivers, then time reversed and retransmitted. The TR idea, which has its roots in optical phase conjugation, has been used in numerous studies in acoustics and electromagnetism [3]–[6], and has potential applications ranging from sensing (radar, acoustics, optics, and so on) to communications [4], [5], [7], [8]. The work of [9] and [10] showed that use of TR can improve target detection.

The TR process can also be repeated multiple times, resulting in signals with certain interesting properties. The lynchpin of this iterative TR approach is the application of the classical mathematical theorem known as the power method, which guarantees that under mild conditions, the application of successive powers of a matrix to an arbitrary seed vector results in a sequence of vectors that converges to the eigenvector associated with the maximum eigenvalue [11]. In the sensing context, the relevant matrix is the frequency-domain TR matrix, which is the product of the scattering matrix and its adjoint. At each frequency, the largest eigenvector (i.e., the eigenvector associated with the largest eigenvalue) corresponds to specifying the relative strengths and phases of the transmitted fields in a way that causes the most energy to scatter back to the receivers. This eigenvector contains information about the scatterers: [2], [12] showed that for noninteracting point-like scatterers, the associated wavefield focuses on the strongest scatterer [13], [14]. For a single spherical target, [15] showed that the largest eigenvector contains information about the target size and composition. In the electromagnetic (EM) case [16], [17], several eigenvalues may be associated with the strongest scatterer.

The power method as described above cannot be used in a straightforward way to predict the shape of the time-domain waveform produced by the iterative TR process. A theory to predict the time-domain behavior was developed in [18] and [19] for the ideal half-space case of sensors covering an infinite plane. These papers showed that the waveform returning the greatest scattered energy can be produced by an iterative TR process, which in general converges automatically to a certain single-frequency waveform. The frequency of this limiting waveform is the strongest resonance, namely the frequency at which the largest eigenvalue attains its maximum, and the waveform's spatial shape (or radiation pattern) is given by the corresponding eigenfunction. Thus, at least in this idealized geometry, [18] and [19] predicted that the time-domain iterative TR process can be used to tune automatically to the space-time waveform that is optimal in the sense of providing the best target detection performance. We emphasize that this tuning takes place without any prior knowledge of the target properties, or even knowledge of whether a target is present.

Manuscript received October 7, 2015; revised May 7, 2016; accepted June 27, 2016. Date of publication July 21, 2016; date of current version October 4, 2016. Cheney was supported by the Air Force Office of Scientific Research under Grant FA9550-14-1-0185, consequently the U.S. Government is authorized to reproduce and distribute reprints for Governmental purposes notwithstanding any copyright notation thereon.

J. Kim was with the Tactical Electronic Warfare Division, U.S. Naval Research Laboratory, Washington, DC 20375 USA, and also with the Rensselaer Polytechnic Institute, Troy, NY 12180 USA (e-mail: jerrykim00@hotmail.com).

M. Cheney is with the Department of Mathematics, Colorado State University, Fort Collins, CO 80523 USA (e-mail: cheney@math.colostate.edu).

E. Mokole, retired, was with the Radar Division, U.S. Naval Research Laboratory, Washington, DC 20375 USA (e-mail: eric.mokole@outlook.com).

Digital Object Identifier 10.1109/TAP.2016.2593718

The predictions of [18] and [19] are consistent with the simulations of [20], which found an approximation to the planar waveform that scatters the greatest energy from a layered medium by discretizing the time-domain problem to obtain a matrix, and then numerically determining the largest eigenvalue of that matrix. They found also that the waveform causing the most scattering is time harmonic.

The corresponding theory for a more realistic sensor geometry has not been studied. However, there are reasons to believe that the same automatic tuning behavior will hold for a limited number of discrete sensors. First, Prada *et al.* [2], Fink and Prada [4], Fink [13], Kyritsi and Papanicolaou [21], and Montaldo *et al.* [22] found that in their acoustic experiments, as the iterative TR process proceeds, the oscillatory pulse lengthens (acquires more oscillations) and the frequency can shift. Second, the tuning predictions were explicitly tested in single-sensor sonar experiments reported in [23], where the authors proposed that target detection could be based on whether the iterative TR process found a resonant frequency.

Even though a variety of authors, e.g., [10], and [24] have considered wideband waveforms and realistic sensor geometries in the analysis of various TR properties, these studies have not addressed the issue of frequency-tuning behavior of the iterative TR process. This gap in the literature can probably be traced to the fact that much of the work on scattering makes the single-scattering approximation or Born approximation. In other words, rays emanating from the transmitter are assumed to bounce only once off the target and then return directly to the receiver. The Born approximation has the advantage of providing a simple closed-form approximate expression for the scattered field, but because it neglects multiple scattering (multiple bounces) and therefore the effect of frequency-dependent constructive interference, the Born approximation predicts that the frequency dependence of the scattering is trivial. In this paper, we do not make the Born approximation. Instead we include the full multiple scattering processes needed to model scattering from a complex target. No frequency-tuning theory for a multiply scattering target and realistic sensor geometry can be found in the literature.

This paper develops such a theory for the case of two sensors and an isolated, multiply scattering target in free space. Throughout we consider only the simplest possible target involving multiple scattering, namely two interacting point-like scatterers. We develop the theory for this simple special case in order to show explicit formulas for the scattering operator and the associated resonances. However, the theory can easily be extended to more complex targets and different numbers of sensors.

The theory we develop for the two-sensor geometry shows that an iterative TR algorithm can be used to tune automatically to the strongest target resonance present in the system's frequency passband. In addition, we investigate the behavior of the iterative TR process for a small number of iterations and are able to obtain not only the largest resonance, as suggested by the idealized theory [18], [19], but also all the resonances within the system's frequency passband, a result which is also new. Moreover, the TR process for finding resonances is a stable method. We contrast this with the process of finding the resonances from the scattering matrix, a process that can be unstable.

We show, in addition, that the frequency-tuning behavior of the iterative TR process has connections with the singularity expansion method (SEM) [25]. Specifically, the poles of the SEM, which appear in the expression for the scattered field, are associated with the resonances derived from the iterative TR process. The SEM process proposes extracting resonances from the large-time asymptotic behavior of the scattered field. This idea also appears in [24], which suggests obtaining resonances from the large-time asymptotic behavior of the TR matrix.

We note that the iterative TR process discussed here is distinct from the imaging algorithm TR-MUSIC [26], [27], in which the MUSIC imaging scheme [28] is applied to the multistatic response matrix or scattering operator. The iterative TR process is also distinct from the method called Décomposition de l'Opérateur de Retournement Temporel, which involves a singular value decomposition of the TR matrix. Since we address detection rather than imaging, we also do not address issues of resolution.

Our focus is also distinct from the very interesting work involving the TR process in multiply scattering dispersive environments [29], [30] in two respects: 1) our targets are in free space and 2) our targets involve multiple scattering (no Born approximation).

This paper is organized as follows. In Section II, we provide some mathematical background on scattering theory and carry out the Foldy–Lax method [31] to obtain the scattering operator for the case of two point scatterers and two transmit/receive pairs. In Section III, we obtain explicit analytical expressions for the scattering operator and its spectral decomposition. In Section IV, we outline the TR process and discuss its behavior in the two-target, two-sensor case. In Section V, we discuss the connection to the SEM poles. In Section VI, we discuss the stability of the iterative TR process. In Section VII, we show simulation results. Section VIII gives conclusions and suggestions for future work.

II. Mathematical Formulation and Derivation

We use the simplified scalar model of the wave equation for the time-domain electric field E at position $\mathbf{r}$

$$\left(\nabla^2 - \frac{1}{c^2(\mathbf{r})}\frac{\partial^2}{\partial t^2}\right) E(\mathbf{r},t) = F(\mathbf{r},t) \tag{1}$$

where F denotes the radiation source, and where we think of $c(\mathbf{r})$ as the local speed of propagation of the EM waves in a specified medium. In free space, the speed is c_0.

We use the Fourier transform

$$\tilde{E}(\mathbf{r},\omega) = \int_{-\infty}^{\infty} E_{\text{tot}}(\mathbf{r},t)e^{-j\omega t}\,dt \tag{2}$$

to write (1) as

$$(\nabla^2 + k^2 + \omega^2 V(\mathbf{r}))\tilde{E}_{\text{tot}}(\mathbf{r},\omega) = \tilde{F}(\mathbf{r},\omega) \tag{3}$$

where $k = \omega/c_0$ and

$$V(\mathbf{r}) = \frac{1}{c^2(\mathbf{r})} - \frac{1}{c_0^2}. \tag{4}$$

The convention throughout is that a tilde denotes a frequency-domain quantity.

When $V = 0$, the solution to (3) is [32]

$$\tilde{E}_{\text{in}}(\mathbf{r}, \omega) = \int \tilde{G}(\mathbf{r} - \mathbf{y}, \omega)\tilde{F}(\mathbf{y}, \omega)\, d\mathbf{y} \tag{5}$$

where $\tilde{G}$ is the outgoing Green's function for $-(\nabla^2 + k^2)$, namely

$$\tilde{G}(\mathbf{r}, \omega) = \frac{e^{-jk\|\mathbf{r}\|}}{4\pi\|\mathbf{r}\|} \tag{6}$$

where $\|\cdot\|$ is the Euclidean norm.

We can write the total field as a sum of the incident field in (5) plus the scattered field generated by a target: $\tilde{E}_{\text{tot}} = \tilde{E}_{\text{in}} + \tilde{E}_{\text{sc}}$ [32]. Subtracting the equation for $\tilde{E}_{\text{in}}$ [the $V = 0$ version of (3)] from (3) yields

$$(\nabla^2 + k^2)\tilde{E}_{\text{sc}}(\mathbf{r}, \omega) = -V(\mathbf{r})\omega^2\tilde{E}_{\text{tot}}(\mathbf{r}, \omega). \tag{7}$$

In this paper, we consider the special case of two transmit/receive sensors located at $\mathbf{y}_1$ and $\mathbf{y}_2$ and a target consisting of two interacting point scatterers located at $\mathbf{x}_1$ and $\mathbf{x}_2$. In this case, (4) becomes

$$V(\mathbf{r}) = \sum_{m=1}^{2} q_m \delta(\mathbf{r} - \mathbf{x}_m) \tag{8}$$

where q_m is the scattering strength or the reflectivity of the mth scatterer.

We use the Foldy–Lax method [28], [31] to obtain an explicit expression for the scattered field. With the notation $\mathbf{d} = \mathbf{x}_1 - \mathbf{x}_2$, the result is (see Appendix A)

$$\begin{aligned}\tilde{E}_{\text{sc}}(\mathbf{r}, \omega) = {} & \omega^2 q_1 \tilde{G}(\mathbf{r} - \mathbf{x}_1) \\ & \times \frac{\tilde{E}_{\text{in}}(\mathbf{x}_1, \omega) + \omega^2 q_2 \tilde{G}(\mathbf{d})\tilde{E}_{\text{in}}(\mathbf{x}_2, \omega)}{1 - \omega^4 q_1 q_2 \tilde{G}^2(\mathbf{d})} \\ & + \omega^2 q_2 \tilde{G}(\mathbf{r} - \mathbf{x}_2) \\ & \times \frac{\tilde{E}_{\text{in}}(\mathbf{x}_2, \omega) + \omega^2 q_1 \tilde{G}(\mathbf{d})\tilde{E}_{\text{in}}(\mathbf{x}_1, \omega)}{1 - \omega^4 q_1 q_2 \tilde{G}^2(\mathbf{d})}.\end{aligned} \tag{9}$$

Note that when $\omega^4 q_1 q_2 \tilde{G}^2(\mathbf{d}) < 1$, the denominator of (9) can be expanded in a geometric series, and in the resulting expression, each term can be interpreted in terms of scattering and propagation between sensors and scatterers.

In this example, the source in (1) is

$$\tilde{F}(\mathbf{r}, \omega) = \sum_{i=1}^{2} \mu_0 j\omega \tilde{J}_i(\omega)\delta(\mathbf{r} - \mathbf{y}_i)^1 \tag{10}$$

where μ_0 is the permeability of free space, and $\tilde{J}_i$ is the current density of the i^{th} source. Since $\tilde{F}$ is the sum of point-like sources from the transmitter locations $\mathbf{y}_i$, the incident field in (5) is

$$\tilde{E}_{\text{in}}(\mathbf{r}, \omega) = \sum_{i=1}^{2} -\mu_0 j\omega \tilde{J}_i(\omega)\frac{e^{-jk\|\mathbf{r} - \mathbf{y}_i\|}}{4\pi\|\mathbf{r} - \mathbf{y}_i\|}. \tag{11}$$

[1]The units of $\tilde{J}$ are ampere-meters, which is due to the choice of a point-like volume source for our model.

Consequently, the received field is

$$\tilde{\mathbf{R}}(\omega) = \tilde{S}(\omega)\tilde{\mathbf{T}}(\omega) \tag{12}$$

where the transmitted and received signal vectors are

$$\tilde{\mathbf{T}}(\omega) = \begin{bmatrix} \mu_0 j\omega \tilde{J}_1(\omega) \\ \mu_0 j\omega \tilde{J}_2(\omega) \end{bmatrix}, \quad \tilde{\mathbf{R}}(\omega) = \begin{bmatrix} \tilde{R}_1(\omega) \\ \tilde{R}_2(\omega) \end{bmatrix} \tag{13}$$

and the scattering operator is the square matrix

$$\begin{aligned}\tilde{S}_{ik} = {} & \frac{1}{\xi}\sum_{n=1}^{2} \tilde{G}(\mathbf{y}_i - \mathbf{x}_n, \omega)\omega^2 q_n \\ & \times [\tilde{G}(\mathbf{x}_n - \mathbf{y}_k, \omega) + \omega^2 q_{(n \bmod 2)+1}\tilde{G}(\mathbf{d}, \omega) \\ & \times \tilde{G}(\mathbf{x}_{(n \bmod 2)+1} - \mathbf{y}_k, \omega)]\end{aligned} \tag{14}$$

also known as the multistatic data matrix or the transfer matrix. Here

$$\xi = 1 - q_1 q_2 \omega^4 \tilde{G}^2(\mathbf{d}, \omega). \tag{15}$$

If the scattering between the two scatterers is weak, one can assume $\xi \approx 1$. Here, for simplicity, we have assumed that the magnitude of the antenna frequency response is flat in the frequency band of interest.

III. Analysis of the Scattering Matrix

On careful examination, (14) can be expressed as

$$\tilde{S} = \frac{\omega^2}{\xi} P \Delta P^T, \tag{16}$$

the product of two propagator matrices (P and P^T) and an interaction matrix (Δ), where

$$\Delta = \begin{bmatrix} q_1 & q_1 q_2 \omega^2 \tilde{G}(\mathbf{d}, \omega) \\ q_1 q_2 \omega^2 \tilde{G}(\mathbf{d}, \omega) & q_2 \end{bmatrix} \tag{17}$$

$$P = \begin{bmatrix} \tilde{G}(\mathbf{y}_1 - \mathbf{x}_1, \omega) & \tilde{G}(\mathbf{y}_1 - \mathbf{x}_2, \omega) \\ \tilde{G}(\mathbf{y}_2 - \mathbf{x}_1, \omega) & \tilde{G}(\mathbf{y}_2 - \mathbf{x}_2, \omega) \end{bmatrix} \tag{18}$$

and the superscript T denotes matrix transposition. All three matrices are physically interpretable. In particular, P is an operator that maps the fields at the scatterer locations $\mathbf{x}_1$ and $\mathbf{x}_2$ to the corresponding fields at receiver locations $\mathbf{y}_1$ and $\mathbf{y}_2$. The transpose P^T maps the fields from the transmitters located at $\mathbf{y}_1$ and $\mathbf{y}_2$ to the fields at the scatterers. The interaction matrix Δ describes the field interactions due to the scatterers.

The interaction matrix is singular at the frequencies ω_α for which

$$\xi(\omega_\alpha) = 1 - q_1 q_2 \omega_\alpha^4 \tilde{G}^2(\mathbf{d}, \omega_\alpha) = 0. \tag{19}$$

We note also that the interaction matrix Δ is aspect independent; in other words, it does not depend on the spatial relationship between the targets and sensors. Consequently, it could be useful for various applications such as target classification. Unfortunately, the interaction matrix (17) cannot be measured directly; instead the scattering matrix (16) is the measurable quantity. The scattering matrix $\tilde{S}$ depends on the viewing angles between sensors and targets because the propagator matrices (18) do.

One case in which the scattering matrix can be used to obtain information about the scatterers is when the coupling between the scatterers, namely $q_1 q_2 \omega^4 \tilde{G}^2(\mathbf{d}, \omega)$, is weak.

In this case, the off-diagonal elements of Δ are negligible, and $\xi = 1$ from (15). This case was addressed in [12] and [34], which showed that with enough sensors, the nth eigenvalue of the scattering matrix corresponds to the nth strongest point-like scatterer. For extended scatterers, multiple eigenvalues can correspond to a single scatterer, and these eigenvalues provide information about the scatterer [17].

In this paper, we consider the more general case in which there is coupling between the two scatterers; that is, we take into account the effects of multiple scattering between the two scatterers. In this case, the eigenvalues of the scattering operator do not necessarily correspond to individual scatterers. However, [26] and [27] showed that focusing can still be achieved. The primary concern of previous works was to resolve accurate target locations. In contrast, our focus is on the use of TR to obtain resonant frequencies that could potentially be used to identify the target. Below, we discuss the connection between the resonances and the eigenvalues of the TR operator. First, we carry out the following analysis that shows how the eigenvalues of the scattering operator depend on the target characteristics. For notational convenience, we omit explicit references to frequency in the Green's function, eigenvalues, and the operators unless it is required.

A. Spectral Decomposition of Interaction Matrix Δ

The eigenvalues of Δ are

$$\lambda_{1,2} = \frac{(q_1+q_2) \pm \sqrt{(q_1-q_2)^2 + 4(q_1q_2\tilde{G}(\mathbf{d})\omega^2)^2}}{2}, \quad (20)$$

and the corresponding eigenvectors are

$$X_1 = \left[-\frac{-q_1+q_2-\sqrt{(q_1-q_2)^2+4(q_1q_2\tilde{G}(\mathbf{d})\omega^2)^2}}{2\omega^2\tilde{G}(\mathbf{d})q_1q_2} \; 1 \right]^T \quad (21)$$

$$X_2 = \left[-\frac{-q_1+q_2+\sqrt{(q_1-q_2)^2+4(q_1q_2\tilde{G}(\mathbf{d})\omega^2)^2}}{2\omega^2\tilde{G}(\mathbf{d})q_1q_2} \; 1 \right]^T. \quad (22)$$

In the case that $q_1 > q_2$ and $|(4q_1q_2\tilde{G}(\mathbf{d})\omega^2)/((q_1-q_2))^2| < 1$ (multiple scattering is weak), the eigenvalues can be written in a series by using $\sqrt{1+x} = \sum_{n=0}^{\infty}\binom{1/2}{n}x^n$ for $|x| < 1$ to obtain

$$\lambda_1 = q_1 + \sum_{n=1}^{\infty} \frac{q_1-q_2}{2}\binom{1/2}{n}\left(\frac{4q_1q_2\tilde{G}(\mathbf{d})\omega^2}{(q_1-q_2)^2}\right)^n \quad (23)$$

$$\lambda_2 = q_2 - \sum_{n=1}^{\infty} \frac{q_1-q_2}{2}\binom{1/2}{n}\left(\frac{4q_1q_2\tilde{G}(\mathbf{d})\omega^2}{(q_1-q_2)^2}\right)^n. \quad (24)$$

When the higher-order terms in (23) and (24) are negligible, the eigenvalues reduce to

$$\lambda_1 \approx q_1 \quad (25)$$

$$\lambda_2 \approx q_2. \quad (26)$$

Consequently, the eigenvalues of the interaction matrix Δ correspond directly to the scattering strengths when the multiple scattering between the scatterers is weak, which is the case analyzed in [12] and [34].

In the general case, when the interaction between the scatterers cannot be neglected, the interaction matrix can be decomposed into the form

$$\Delta = X\Lambda X^{-1} \quad (27)$$

where X is a matrix whose columns are the eigenvectors $\hat{X}_i = X_i/\|X_i\|$ for $i = 1, 2$, and Λ is a diagonal matrix of the eigenvalues of Δ.

B. Spectral Decomposition of Scattering Matrix $\tilde{S}$

To relate the eigenvalues of $\tilde{S}$ to those of Δ, substitute (27) in (16) to obtain

$$\tilde{S} = \frac{\omega^2}{\xi}(PX)\Lambda(X^{-1}P^T). \quad (28)$$

We determine the eigenvalues γ of $\tilde{S}$ by solving the characteristic equation $\det(\tilde{S} - \gamma I) = 0$, which with (28) becomes

$$0 = \det\left(\frac{\omega^2}{\xi}PX\Lambda X^{-1}P^T - (PX)\gamma I(PX)^{-1}\right)$$
$$\propto \det\left(\frac{\omega^2}{\xi}\Lambda X^{-1}P^T(PX) - \gamma I\right). \quad (29)$$

With the definition $M = X^{-1}P^TPX$, (29) can be written as

$$\det\left(\frac{\omega^2}{\xi}\begin{bmatrix}\lambda_1 m_{11} & \lambda_1 m_{12}\\ \lambda_2 m_{21} & \lambda_2 m_{22}\end{bmatrix} - \gamma I\right) = 0 \quad (30)$$

where m_{ik} is (i,k)th element of matrix M and is explicitly shown in Appendix B.

Because the system is coupled, the contribution from each of the scatterers can be seen in each of the eigenvalues of $\tilde{S}$. Under certain propagation conditions, for example when the off-diagonal elements of M are negligible, the eigenvalues γ of $\tilde{S}$ in (30) can correspond directly to the eigenvalues λ of Δ. In general, however, the relationship is more complicated. The eigenvalues vary in frequency from constructive and destructive interference; an explicit connection to Bragg's law is made in [34], where it is shown that the spacing between the peaks of the maximum eigenvalues is related to the geometry of the sensors and scatterers.

IV. Time-Reversal Process

The iterative TR process [2], [12] involves an array of sensors (possibly distributed) that both transmits and receives. The process is implemented via the following steps.

1) From the mth transmitter, transmit the designated waveform $T_m(t)$ (see below). Thus, the signal transmitted from the sensor array can be written $\mathbf{T}(t) = [T_1(t), T_2(t)]^T$. The transmitted field then scatters from the targets and propagates back to the sensors.
2) The sensors each receive the scattered signal and store it in some manner. The signal received at the nth sensor is

$$R_n(t) = \sum_{m=1}^{2} S_{nm}(t) \star T_m(t) \quad (31)$$

where $\star$ is convolution in time and S_{nm} is the inverse Fourier transform of (14).

3) These stored received signals are time reversed to obtain $\mathbf{R}(-t) = [R_1(-t), R_2(-t)]^T$.
4) The process repeats, with the next transmitted waveform being the previous time-reversed received signal: $\mathbf{T}(t) = \mathbf{R}(-t)$.

Moreover, the time-reversed received signal vector is the phase conjugate of the received signal $\tilde{\mathbf{R}}$. After $2n$ and $2n+1$ repetitions, respectively, the results are

$$\tilde{\mathbf{T}}^{2n}(\omega) = (\tilde{S}^*\tilde{S})^n\tilde{\mathbf{T}}^0(\omega)$$
$$\tilde{\mathbf{T}}^{2n+1}(\omega) = (\tilde{S}^*\tilde{S})^n\tilde{S}^*\tilde{\mathbf{T}}^{0*}(\omega) \tag{32}$$

where the superscript $*$ denotes complex conjugate. Fink [3] and Fink and Prada [4] showed that for each frequency, the power method [11] governs this process. Thus, with any choice of initial nonzero vector $\tilde{\mathbf{T}}^0$ and appropriate normalization, the sequence of vectors $\tilde{\mathbf{T}}^{2n}$ converges to the eigenvector of $\tilde{S}^*\tilde{S}$ associated with the largest eigenvalue, provided that this largest eigenvalue is not degenerate. If the largest eigenvalue is degenerate, the process still provides a vector in the eigenspace associated with the largest eigenvalue.

Experiments [2] typically do not use a waveform consisting of a single frequency; thus, the question arises of how to analyze the TR process in the time domain. Cheney *et al.* [18], [19] showed that in an idealized half-space problem, the time-domain iterative TR process converges in general to a single time-harmonic wave; in other words, at least in the half-space geometry, with infinitely many sensors, the TR process sharpens peaks in the spectrum. Therefore, the iterative TR process produces a spectrum with peaks at the resonant frequencies. Below, we show that this phenomenon occurs also in the more realistic example in which only two sensors are used.

The fact that the iterative TR process can be used to find the resonant frequencies suggests a connection with the SEM [25].

V. Connection to SEM

Baum [25], [35] first introduced SEM in the context of EM scatterers and antennas. His approach to modeling the scattered field in terms of poles was originally motivated by the observation of typical transient responses of complex scatterers. He conjectured that the responses were dominated by several damped sinusoids, and his main focus was scatterers on which the incident field creates surface current densities. These densities can be analyzed in terms of the object's natural frequencies ω_α [25], which typically occur at complex (non-physical) values. In particular, each component of the scattering matrix $\tilde{S}$ is a meromorphic function of ω, where the poles $\{\omega_{\alpha_k}\}_{k=1}^{\infty}$ satisfy $\xi = 1 - q_1q_2\omega_{\alpha_k}^4\tilde{G}^2(\mathbf{d}, \omega_{\alpha_k}) = 0$ and are put in order of increasing imaginary part. Thus, the scattering matrix $\tilde{S}(\omega)$ can be expanded in a Laurent series around a given pole ω_{α_k}

$$\tilde{S}(\omega) = \sum_{n=-m}^{\infty} s_n(\omega_{\alpha_k})(\omega - \omega_{\alpha_k})^n \tag{33}$$

where m is a positive integer, and s_n is a matrix consisting of the residues of the elements of $\tilde{S}(\omega)$ at ω_{α_k}.

When the transmitted waveform $\tilde{\mathbf{T}}(\omega)$ is analytic, then $\tilde{\mathbf{R}}(\omega)$ is meromorphic. Moreover, both $\mathbf{T}(t)$ and $\mathbf{R}(t)$ must be causal ($\mathbf{T}(t) = \mathbf{0} = \mathbf{R}(t)$ for $t < 0$). By the Paley–Wiener theorem [36, p. 494], both $\tilde{\mathbf{T}}(\omega)$ and $\tilde{\mathbf{R}}(\omega)$ are then analytic in the lower half plane. Consequently, the poles of the $\tilde{\mathbf{R}}(\omega)$ must lie in the upper half plane. Using the Paley–Wiener theorem allows one to avoid the convergence issues inherent in Baum's Laplace formulation.

To predict the time-domain received signal, one must compute the inverse Fourier transform for the received signal, which may require modification of the integration contour. By an appropriate contour deformation and by residue calculus, we obtain

$$\mathbf{R}(t) \approx 2\pi j \sum_{i=1}^{N} \operatorname*{Res}_{\omega=\omega_{\alpha_i}} \left(\frac{\tilde{\mathbf{R}}(\omega)e^{j\omega t}}{2\pi} \right) + O(e^{-|\mathrm{Im}(\omega_{\alpha_N})|t}), \tag{34}$$

where the higher-order terms vanish as $t \to \infty$, and the notation $f(x) = O(g(x))$ means that $|f(x)| \le M|g(x)|$ for some positive real number M as $x \to \infty$. Equation (34) is the SEM representation of the transient backscattered response at the receivers [35], [37].

We note that the poles of (16) due to ξ are a result of the interaction between the fields and scatterers. These poles are aspect independent, and it is for this reason that they have been proposed for use in target classification [38]. Consequently, a number of methods, such as the matrix-pencil method and Prony's method, have been developed for determining these poles [39]–[43]. Unfortunately, the problem of obtaining these poles from real data is ill-posed and sensitive to noise. Previous research [44], [45] has shown, however, that there is a connection between the eigenvalues of the scattering matrix and the complex poles used for Baum's SEM. Although the SEM poles are aspect independent, unfortunately the scattering matrix itself and consequently the received signals are aspect dependent.

We show below that the TR matrix can be used to obtain certain information about the poles of $\tilde{S}$ in a stable manner. First, we introduce the notation $\hat{S} = P\Delta P^T$, so that from (16), $\hat{S}$ is related to $\tilde{S}$ by $\tilde{S} = (\omega^2/\xi)\hat{S}$. From the definition of $\hat{S}$, we have

$$\det(\hat{S}(\omega)) = \det(P(\omega)) \underbrace{\det(\Delta(\omega))}_{q_1q_2\xi(\omega)} \det(P^T(\omega)). \tag{35}$$

The corresponding modified TR matrix $\hat{L}$ is

$$\hat{L} = \hat{S}^\dagger\hat{S}, \quad L = \left|\frac{\omega^2}{\xi}\right|^2 \hat{L}. \tag{36}$$

From (19), at a natural frequency $\omega = \omega_\alpha$, $\xi(\omega_\alpha) = 0$; from (35), we see that the determinant of $\hat{S}$ and therefore also of $\hat{L}$ must be zero, implying that at least one of the eigenvalues of $\hat{S}$ and $\hat{L}$ must be 0. As $\omega \to \omega_\alpha$ and $\xi \to 0$, the eigenvalues of the interaction matrix Δ can be approximated from (20) by

$$\lim_{\omega\to\omega_\alpha} \lambda_1(\omega) \approx q_1 + q_2 \tag{37}$$

$$\lim_{\omega\to\omega_\alpha} \lambda_2(\omega) \approx \frac{q_1q_2}{q_1+q_2}\xi. \tag{38}$$

From (56) in Appendix B, the eigenvalues of $\tilde{S}$ behave as

$$\lim_{\omega\to\omega_\alpha}\gamma_1(\omega) \approx \lim_{\omega\to\omega_\alpha}\frac{\omega^2}{\xi}\lambda_1 m_{11} = \frac{\omega_\alpha^2}{\xi}(q_1+q_2)m_{11} \tag{39}$$

$$\lim_{\omega\to\omega_\alpha}\gamma_2(\omega) \approx \lim_{\omega\to\omega_\alpha}\frac{\omega^2}{\xi}\lambda_2 m_{22} = \frac{\omega_\alpha^2 q_1 q_2}{q_1+q_2}m_{22}. \tag{40}$$

Clearly, γ_1 diverges as $\xi \to 0$, while γ_2 converges to $\omega_\alpha^2 q_1 q_2 m_{22}/(q_1+q_2)$.

We determine the eigenvalues of the TR matrix L from $\{\gamma_1, \gamma_2\}$ by (60) in Appendix C. Consequently, the eigenvalues of L behave as

$$\lim_{\omega\to\omega_\alpha}\sigma_1 = \left(\frac{\omega_\alpha^2}{\xi}(q_1+q_2)m_{11}\frac{(\mathbf{v}_1^*,\mathbf{y}_1)}{(\mathbf{v}_1,\mathbf{y}_1)}\right)^2 \tag{41}$$

$$\lim_{\omega\to\omega_\alpha}\sigma_2 = \left(\frac{\omega_\alpha^2 q_1 q_2 m_{22}(\mathbf{v}_2^*,\mathbf{y}_2)}{(q_1+u_2)(\mathbf{v}_2,\mathbf{y}_2)}\right)^2 \tag{42}$$

where $\mathbf{v}_i$ is an eigenvector of L for σ_i and $\mathbf{y}_i$ is an eigenvector of $\tilde{S}$ for γ_i. Clearly, the larger eigenvalue of L diverges to positive infinity in the limit $\omega \to \omega_\alpha$, while the smaller eigenvalue σ_2 converges to a finite number. Because in general the natural frequencies ω_{α_k} are complex-valued, the larger eigenvalue does not actually diverge for real frequencies, and instead one sees resonance peaks.

When the damping is small [$\mathrm{Im}(\omega_\alpha) \ll 1$], the real resonant frequency is approximately equal to the complex natural frequency, and one expects a significant response at this frequency. The difference between a real resonant frequency ω_α and its associated complex natural frequency depends on the phase of ω_α.

Thus, the TR algorithm provides information about the rotation of the natural frequencies ω_{α_k} onto the real axis. Moreover, we show in Section VI that this information can be obtained in a stable manner. Therefore, the TR algorithm provides a stable way of obtaining information about the SEM poles.

VI. Stability of Eigenvalues

In this section, we compare and contrast the eigenvalues of $\tilde{S}$ and L and show how these eigenvalues are respectively perturbed by noise.

A. Stability of Finding Eigenvalues From Measurements of $\tilde{S}$

Thermal noise gives rise to perturbations in the elements of the scattering matrix. We would like to examine how a small change $\delta\tilde{S}$ in the scattering matrix is translated to the changes $\delta\Gamma$ in the eigenvalues of $\tilde{S}$. The eigendecomposition of $\tilde{S}$ can be written

$$Y^{-1}\tilde{S}Y = \Gamma \tag{43}$$

where Y is a matrix whose columns are the eigenvectors of $\tilde{S}$. Inserting $\Gamma+\delta\Gamma$ and $\tilde{S}+\delta\tilde{S}$ into (43) and rearranging, we have

$$\delta\Gamma = Y^{-1}\delta\tilde{S}Y. \tag{44}$$

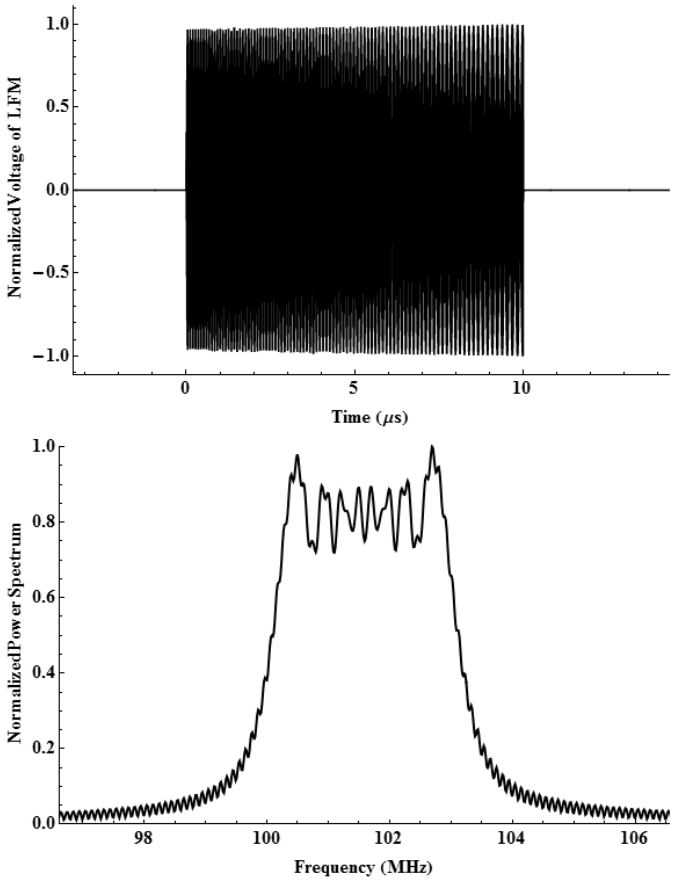

Fig. 1. Original LFM signal T^0: time-domain signal (top) and normalized square magnitude of power spectrum (bottom) with 4-MHz bandwidth centered at 100 MHz.

Taking the operator norm $\|\cdot\|$ and applying a standard matrix product inequality yield

$$\|\delta\Gamma\| = \|Y^{-1}\delta\tilde{S}Y\| \le \|Y^{-1}\|\|\delta\tilde{S}\|\|Y\|. \tag{45}$$

The error is then bounded by

$$\max_\omega \|\delta\Gamma\| \le \|Y^{-1}\|\|Y\|\|\delta\tilde{S}\| = \max_\omega \kappa(Y)\|\delta\tilde{S}\| \tag{46}$$

where κ is the condition number. The errors in the eigenvalues are thus bounded by the errors in the measurements introduced in $\tilde{S}$ and the conditioning of the eigenvectors of $\tilde{S}$ (columns of Y). Since Y depends on the field propagation paths and scattering, the conditioning is a function of frequency and the configuration of the transmitters, receivers, and scatterers. In general, finding the eigenvalues of $\tilde{S}$ from measurements of $\tilde{S}$ is an unstable process.

B. Stability of Finding Eigenvalues From TR Measurements

For the TR operator, the errors in the eigenvalues are less subject to the configuration of the system. From the eigendecomposition $L = V\Sigma V^\dagger$, we have

$$\max_\omega \|\delta\Sigma\| \le \|V\|\|V^\dagger\|\|\delta L\|. \tag{47}$$

Since V is unitary, the norms are both 1. Thus, the estimate corresponding to (46) is

$$\max_\omega \|\delta\Sigma\| \le \max_\omega \|\delta L\|. \tag{48}$$

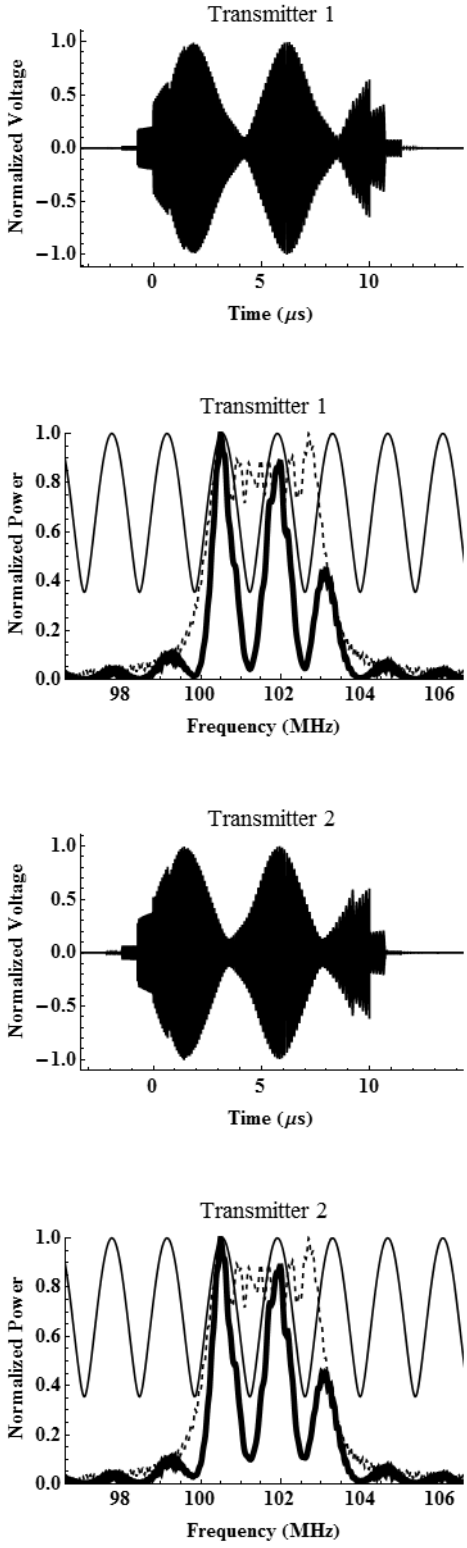

Fig. 2. Top two plots show the normalized transmitted waveform and the power spectrum of sensor 1 after two iterations of the TR algorithm. Bottom two plots show the normalized transmitted waveform and power spectrum of sensor 2 after two iterations. The original LFM (dotted line), the normalized power spectrum of the signal (thick line), and the normalized calculated eigenvalues (thin line) are shown. Scatterers are 500 m apart.

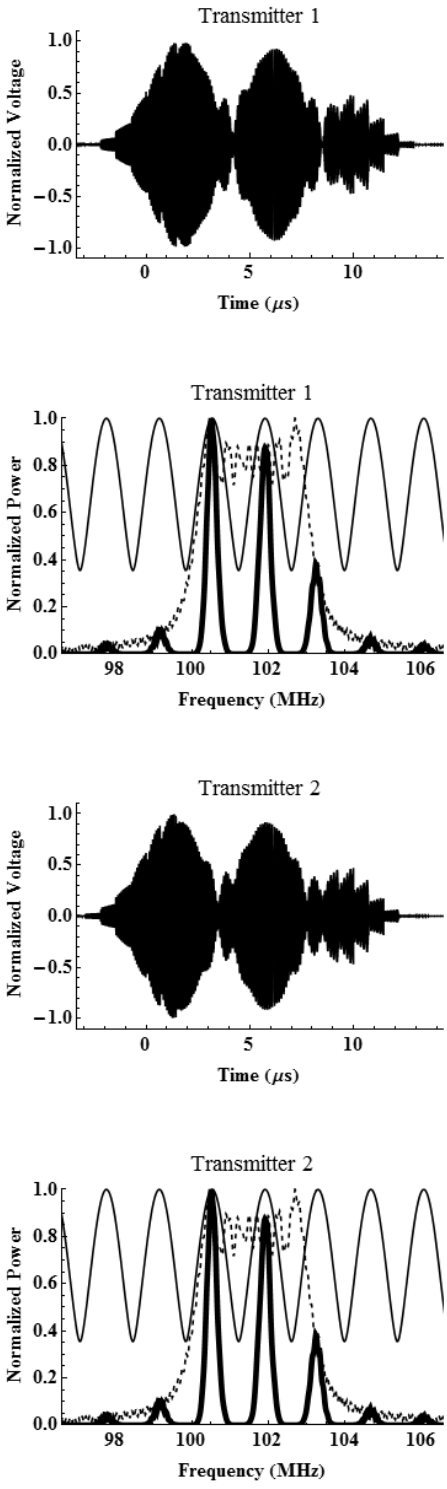

Fig. 3. Top two plots show the normalized transmitted waveform and the power spectrum of sensor 1 after ten iterations of the TR algorithm. Bottom two plots show the normalized transmitted waveform and power spectrum of sensor 2 after ten iterations. The original LFM (dotted line), the normalized power spectrum of the signal (thick line), and the normalized calculated eigenvalues (thin line) are shown. Scatterers are 500 m apart.

The error in the eigenvalues of L does not depend on the conditioning of Y. The error bound in (48) suggests that finding the eigenvalues of the TR operator is a more well-conditioned problem than finding the eigenvalues of the scattering operator.

The iterative TR method, however, does not directly measure the TR operator L. Rather, the local maxima of the largest

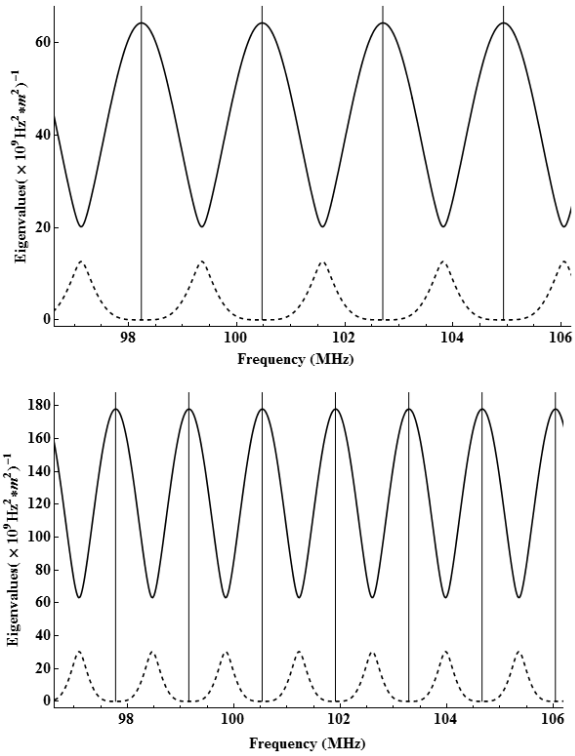

Fig. 4. First and second eigenvalues of the TR matrix L are shown at two separate distances of the point scatterers, 300 m (top) and 500 m (bottom), respectively, with the transmitter and stronger scatterer in the same position. The two figures shown are the theoretical eigenvalues—larger eigenvalue (solid line), smaller eigenvalue (dashed line), and the vertical lines indicate the Bragg frequencies.

eigenvalue are obtained automatically by the TR iterations, whose analysis reduces to that of the power method. Stability of the power method with noisy measurements was established in [46].

VII. Numerical Results

In this section, we provide simulations of the TR algorithm for two transmitter/receiver pairs and two isotropic scatterers in free space. The two transmit/receive pairs are placed at coordinates (−500, 700, 10 m) and (−500, 1000, 10 m). The scatterers are separated by 500 m, with the strong one (q_1) located at (150, 850, 10 m) and the weaker one (q_2) located at (−107.52, 1278.58, 10 m). In addition, the transmitter/receiver pairs and the scatterers are placed in a plane with $q_1 = 0.75$ and $q_2 = 0.4$ Hz^{-2}m^{-2}. The initial waveform $T^0(t)$ for each transmitter is the same linear frequency modulated (LFM) signal with the following characteristics:

1) 10 μs pulse duration;
2) 10^{12} s^{-2} chirp rate;
3) 100 MHz carrier frequency.

For the simulations, we limit ourselves to the even iterations of the transmitted signal. We normalize the signal vector with the euclidean norm (power) for each iteration. We observe the transformation of the original chirp to the final waveform in the time domain and the square magnitude of the power spectrum of the signal. For plotting purposes only, all the power spectra and time-domain waveforms are scaled to have a maximum

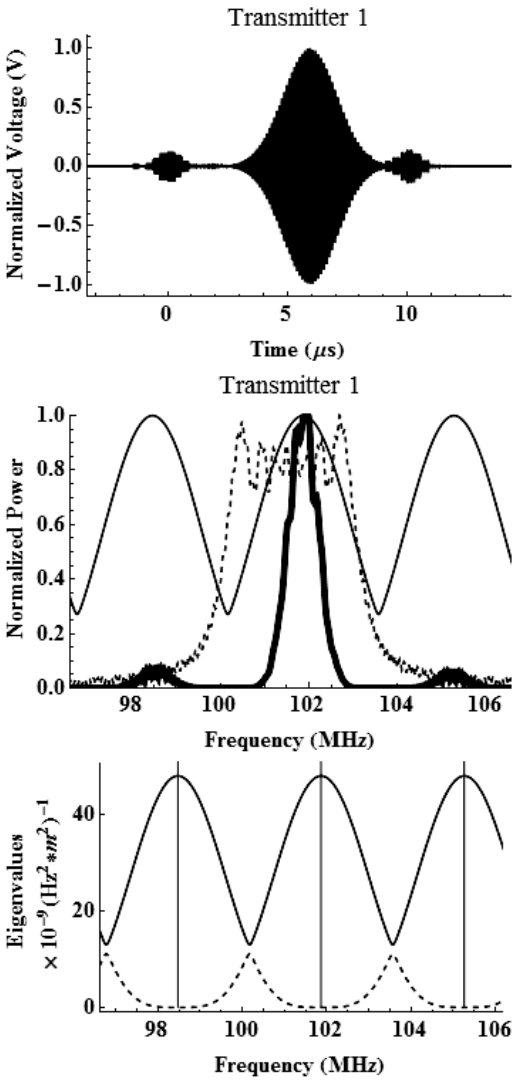

Fig. 5. Scatterers rotated 81° in azimuth from the initial configuration. d remains the same. The eigenvalue peaks are 3.39 MHz apart. TR process was taken out to ten iterations. Top plot is the time-domain signal, middle plot is the power spectrum, and bottom plot is the first (solid line) and second eigenvalues (dashed line) of the TR matrix.

of unity. Fig. 1 shows the original LFM signal to be used in the TR process.

Fig. 2 shows the final waveform from T^0 after two iterations of the TR process, the normalized magnitude of the spectra for TR-generated signals, and the normalized calculated eigenvalues of L for a scatterer separation of 500 m. As Fig. 2 indicates, the time-domain waveform significantly changes and broadens from the original LFM signal for both transmitters. The power spectrum of each new waveform has relative maximum values at the resonant frequencies. Observe that for a given bandwidth of the original LFM signal, the energy of the TR-generated signals after two iterations (thick line) concentrates near the resonant frequencies. Significantly, the maxima of this power spectrum aligns with the maxima of the calculated eigenvalues of the TR operator (thin line). The peaks of the power spectrum occur within the bandwidth of the power spectrum of T^0 (dashed curve).

At higher iterations of the TR process, the field intensities increase at the resonant frequencies and decrease at

other frequencies. In particular, Fig. 3 plots the power spectrum and the time-domain signal at ten iterations. The frequency peaks are sharp, and one can observe the key resonating frequency where the intensity is at its highest. The time-domain waveform has broadened from the 10-μs pulse in Fig. 1 as the new waveform is determined by the resonant frequencies. The plot of the power of the original LFM signal is now narrowed and centered around the resonant frequencies. The largest intensity is found within the bandwidth of the original signal.

Fig. 4 shows the large and small eigenvalues. As discussed in Section V, the larger eigenvalues attain relative maximum values at resonance. The vertical lines indicate the frequencies at which maximal constructive interference occurs. These frequencies match the eigenvalue peaks which are 1.37 MHz apart. This frequency separation corresponds to the projected distance between the scatterers, where the projection is onto the axis normal to the axis vector from the scatterers to the midpoint of the sensors. In this case, the actual distance between the scatterers is 500 m ($= d$), and the projected distance is 484 m. For both scatterer separations in Fig. 4, the larger eigenvalue has a maximum at the resonance frequencies.

In Fig. 5, the weaker scatterer is rotated 81° in azimuth about the stronger scatterer from the original configuration. The projected distance is 197 m. The scatterer separation distance of 500 m remains the same, but the separation between frequency peaks changes to 3.39 MHz. As the projected distance decreases, the eigenvalue peaks will be further apart. A signal with a broader bandwidth will be required to observe multiple resonant peaks. Thus, the aspect angle, which determines the propagation paths of the fields, has a strong influence on the locations of the eigenvalue peaks.

VIII. Conclusion

This paper shows that the TR process provides a stable way of finding the resonances of a scattering system from a small number of sensors. This result is consistent with the findings of [18] and [19], which showed, for an idealized half-space scattering geometry, the TR algorithm automatically converges to the space-time waveform that maximizes the energy scattered back to the receivers. Furthermore, this paper shows that the same result holds for a more realistic sensing system. Thus, the best waveform for target detection is a single harmonic waveform at one of the resonance frequencies, and the TR process provides an automatic, stable method to find these resonance frequencies. We have shown that for finding the eigenvalues (and hence the resonance frequencies), use of the TR process is more stable than use of the scattering matrix itself.

Although our analysis has considered only the simplest possible example of a multiply scattering target, we expect that similar results would hold for extended targets in which multiple scattering is an important effect.

We have shown, moreover, that these scattering system resonances are closely related to the poles of the SEM. In particular, as the poles of the SEM approach the real axis, the SEM poles become exactly the resonances found by the TR process. The precise nature of the information about the SEM poles that is provided by the TR process is a question we leave for future work. Other interesting topics for future work include development of related theory for the case of propagation through lossy and/or dispersive materials.

Appendix A
Derivation of the Scattering Matrix

By convolving both sides of (7) with $\tilde{G}$, we obtain the Lippmann–Schwinger equation for the scattered field at an arbitrary observation point $\mathbf{r}$

$$\tilde{E}_{\text{sc}}(\mathbf{r},\omega) = \int_{\Omega} \tilde{G}(\mathbf{r}-\mathbf{y},\omega)\omega^2 V(\mathbf{y})\tilde{E}_{\text{tot}}(\mathbf{y},\omega)\,d\mathbf{y}. \quad (49)$$

We apply the Foldy–Lax method to model $\tilde{E}_{\text{tot}}$ to determine the scattered field $\tilde{E}_{\text{sc}}$. The Foldy–Lax method [28], [31] requires solving the set of linear equations ($n = 1, 2$)

$$\tilde{E}^n(\mathbf{x}_n,\omega) = \tilde{E}_{\text{in}}(\mathbf{x}_n,\omega) + \sum_{m\neq n} \tilde{G}(\mathbf{x}_n-\mathbf{x}_m,\omega)\omega^2 q_m \tilde{E}^m(\mathbf{x}_m,\omega). \quad (50)$$

Here, $\tilde{E}^m$ denotes the locally incident field at the scatterer m, namely the incident field seen by the mth scatterer. Equation (50) expresses the incident field at the scattering location $\mathbf{x}_n$ as a sum of the overall incident field $\tilde{E}_{\text{in}}$ plus the sum of the scattered fields from all of the other scatterers.

The solution to (50) is

$$\tilde{E}^1(\mathbf{x}_1,\omega) = \frac{\tilde{E}_{\text{in}}(\mathbf{x}_1,\omega) + q_2\omega^2\tilde{G}(\mathbf{d})\tilde{E}_{\text{in}}(\mathbf{x}_2,\omega)}{1-\omega^4 q_1 q_2 \tilde{G}^2(\mathbf{d})} \quad (51)$$

$$\tilde{E}^2(\mathbf{x}_2,\omega) = \frac{\tilde{E}_{\text{in}}(\mathbf{x}_2,\omega) + q_1\omega^2\tilde{G}(\mathbf{d})\tilde{E}_{\text{in}}(\mathbf{x}_1,\omega)}{1-\omega^4 q_1 q_2 \tilde{G}^2(\mathbf{d})} \quad (52)$$

where $\mathbf{d} = \mathbf{x}_1 - \mathbf{x}_2$ and where for notational convenience, we have suppressed the ω argument in $\tilde{G}$.

In (49), we use (8) and substitute the locally incident field (51) for the total field $\tilde{E}_{\text{tot}}$ at the appropriate scatterer. The scattered field is then

$$\tilde{E}_{\text{sc}}(\mathbf{r},\omega) = \sum_{m=1}^{2} \tilde{G}(\mathbf{r}-\mathbf{x}_m,\omega)\omega^2 q_m \tilde{E}^m(\mathbf{x}_m,\omega). \quad (53)$$

Equation (53) expresses the overall scattered field at some observation point $\mathbf{r}$ as a sum of scattered fields from each scatterer.

Appendix B
Derivation of the Eigenvalues of the Scattering Matrix $\tilde{a}$

The characteristic polynomial of (29) can be expressed as

$$\det\left(\frac{\omega^2}{\xi}\Lambda M - \gamma I\right) = 0 \quad (54)$$

$$\Lambda = \begin{bmatrix} \lambda_1 & 0 \\ 0 & \lambda_2 \end{bmatrix}, \quad M = X^{-1}P^T P X = \begin{bmatrix} m_{11} & m_{12} \\ m_{21} & m_{22} \end{bmatrix} \quad (55)$$

whose solutions are

$$\gamma_{1,2} = \frac{\omega^2}{\xi} \times \left(\frac{\lambda_1 m_{11} + \lambda_2 m_{22}}{2} \pm \frac{\sqrt{(\lambda_1 m_{11} - \lambda_2 m_{22})^2 + 4\lambda_1 \lambda_2 m_{21} m_{12}}}{2} \right). \tag{56}$$

APPENDIX C
RELATIONSHIP BETWEEN SINGULAR VALUES OF THE SCATTERING OPERATOR $\tilde{S}$ AND THE EIGENVALUES OF THE TR OPERATOR L

Any matrix $\tilde{S}$ has a singular value decomposition

$$\tilde{S} = U \Sigma V^{\dagger} \tag{57}$$

where U and V are unitary matrices. If we multiply (57) by the adjoint $\tilde{S}^{\dagger}$, then we have $L = \tilde{S}^{\dagger}\tilde{S} = V\Sigma^{\dagger}U^{\dagger}U\Sigma V^{\dagger} = V\Sigma^2 V^{\dagger}$, and then post-multiplying V on both sides implies $\tilde{S}^{\dagger}\tilde{S}V = V\Sigma^2$. Therefore, the right singular vectors of $\tilde{S}$ are the eigenvectors of $L = \tilde{S}^{\dagger}\tilde{S}$, and the eigenvalues $\{\sigma_1, \sigma_2\}$ of L are the squares of the corresponding singular values $\{\zeta_1, \zeta_2\}$ of $\tilde{S}$.

For a square matrix with distinct singular values, the left and right singular vectors are unique up to a complex sign (i.e., complex scalar factors of absolute value unity) [47, p. 29]. Since $\tilde{S}$ is square and symmetric but not self-adjoint, the left singular vectors are the conjugates of the right singular vectors: $V^*\Sigma U^T = \tilde{S}^T = \tilde{S} = U\Sigma V^{\dagger}$. Therefore $U = V^*$, which implies that for any right singular vector $\mathbf{v}_l$, there is a left singular vector $\mathbf{u}_l$ such that

$$\tilde{S}\mathbf{v}_l = \zeta_l \mathbf{u}_l = \zeta_l \mathbf{v}_l^*. \tag{58}$$

The inner product of $L\mathbf{v}_l$ with an eigenvector $\mathbf{y}_n$ of $\tilde{S}$ corresponding to the eigenvalue γ_n is

$$\sigma_l(\mathbf{v}_l, \mathbf{y}_n) = (L\mathbf{v}_l, \mathbf{y}_n) = (\tilde{S}^{\dagger}\tilde{S}\mathbf{v}_l, \mathbf{y}_n) = (\tilde{S}\mathbf{v}_l, \tilde{S}\mathbf{y}_n) \tag{59}$$

where $\zeta_l^2 = \sigma_l$. In (59), we use expression (58) for $\tilde{S}\mathbf{v}_l$ and the relation $\tilde{S}\mathbf{y}_n = \gamma_n \mathbf{y}_n$ to obtain $\sigma_l(\mathbf{v}_l, \mathbf{y}_n) = \zeta_l \gamma_n (\mathbf{v}_l^*, \mathbf{y}_n)$. Since $\sqrt{\sigma_l} = \zeta_l$

$$\sqrt{\sigma_l} = \gamma_n \frac{(\mathbf{v}_l^*, \mathbf{y}_n)}{(\mathbf{v}_l, \mathbf{y}_n)}. \tag{60}$$

ACKNOWLEDGMENT

The authors would like to thank Dr. S. Hong from the Rose-Hulman Institute of Technology and Dr. T. Andreadis from the Tactical Electronics Warfare Division for their comments, feedback, and support of this paper. They would also like to thank Dr. S. Blunt from the University of Kansas for his inputs and relevant references. The work of J. Kim was performed under the auspices of the Naval Research Laboratory base programs. The views and conclusions contained herein are those of the authors and do not reflect the official policies or endorsements, either expressed or implied, of the Air Force Research Laboratory, the Naval Research Laboratory, the Department of Defense, or the U.S. Government.

REFERENCES

[1] V. Gregers-Hansen, "A sequential logic for improving signal detectability in frequency-agile search radars," *IEEE Trans. Aerosp. Electron. Syst.*, vol. AES-4, no. 5, pp. 763–773, Sep. 1968.
[2] C. Prada, J.-L. Thomas, and M. Fink, "The iterative time reversal process: Analysis of the convergence," *J. Acoust. Soc. Amer.*, vol. 97, no. 1, pp. 62–71, Jan. 1995.
[3] M. Fink, "Time reversal of ultrasonic fields—Part I: Basic principles," *IEEE Trans. Ultrason., Ferroelectr., Freq. Control*, vol. 39, no. 5, pp. 555–566, Sep. 1992.
[4] M. Fink and C. Prada, "Acoustic time-reversal mirrors," *Inverse Problems*, vol. 17, no. 1, pp. R1–R38, 2001.
[5] W. M. G. Dyab, T. K. Sarkar, A. García-Lampérez, M. Salazar-Palma, and M. A. Lagunas, "A critical look at the principles of electromagnetic time reversal and its consequences," *IEEE Antennas Propag. Mag.*, vol. 55, no. 5, pp. 28–62, Oct. 2013.
[6] J. de Rosny, G. Lerosey, and M. Fink, "Theory of electromagnetic time-reversal mirrors," *IEEE Trans. Antennas Propag.*, vol. 58, no. 10, pp. 3139–3149, Oct. 2010.
[7] B. P. Bogert, "Demonstration of delay distortion correction by time-reversal techniques," *IRE Trans. Commun. Syst.*, vol. 5, no. 3, pp. 2–7, Dec. 1957.
[8] H. Tortel, G. Micolau, and M. Saillard, "Decomposition of the time reversal operator for electromagnetic scattering," *J. Electromagn. Waves Appl.*, vol. 13, no. 5, pp. 687–719, 1999.
[9] Y. Jin and J. M. F. Moura, "Time-reversal detection using antenna arrays," *IEEE Trans. Signal Process.*, vol. 57, no. 4, pp. 1396–1414, Apr. 2009.
[10] J. M. F. Moura and Y. Jin, "Detection by time reversal: Single antenna," *IEEE Trans. Signal Process.*, vol. 55, no. 1, pp. 187–201, Jan. 2007.
[11] E. Isaacson and H. B. Keller, *Analysis of Numerical Methods*. New York, NY, USA: Dover, 1966, pp. 147–150.
[12] C. Prada and M. Fink, "Eigenmodes of the time reversal operator: A solution to selective focusing in multiple-target media," *Wave Motion*, vol. 20, no. 2, pp. 151–163, Sep. 1994.
[13] M. Fink, "Time-reversed acoustics," *Sci. Amer.*, vol. 281, no. 5, pp. 91–97, Nov. 1999.
[14] P. Blomgren, G. Papanicolaou, and H. Zhao, "Super-resolution in time-reversal acoustics," *J. Acoust. Soc. Amer.*, vol. 111, no. 1, p. 230, Jan. 2002.
[15] D. H. Chambers and A. K. Gautesen, "Time reversal for a single spherical scatterer," *J. Acoust. Soc. Amer.*, vol. 109, no. 6, pp. 2616–2624, 2001. [Online]. Available: http://scitation.aip.org/content/asa/journal/jasa/109/6/10.1121/1.1368404
[16] D. H. Chambers and J. G. Berryman, "Analysis of the time-reversal operator for a small spherical scatterer in an electromagnetic field," *IEEE Trans. Antennas Propag.*, vol. 52, no. 7, pp. 1729–1738, Jul. 2004.
[17] D. H. Chambers and J. G. Berryman, "Target characterization using decomposition of the time-reversal operator: Electromagnetic scattering from small ellipsoids," *Inverse Prob.*, vol. 22, no. 6, p. 2145, 2006.
[18] M. Cheney, D. Isaacson, and M. Lassas, "Optimal acoustic measurements," *SIAM J. Appl. Math.*, vol. 61, no. 5, pp. 1628–1647, 2001.
[19] M. Cheney and G. Kristensson, "Optimal electromagnetic measurements," *J. Electromagn. Wave*, vol. 15, no. 10, pp. 1323–1336, 2001. [Online]. Available: http://dx.doi.org/10.1163/156939301X01228
[20] E. Cherkaeva and A. Tripp, "On optimal design of transient electromagnetic waveforms," in *Proc. 67th Annu. Meeting Soc. Exploration Geophys. Expanded Abstracts*, 1997, pp. 438–441.
[21] P. Kyritsi and G. Papanicolaou, "Time-reversal: Spatio-temporal focusing and its dependence on channel correlation," in *Proc. Int. Conf. Signal Process. Commun. Syst. (ICSPCS)*, 2007, pp. 17–19.
[22] G. Montaldo, M. Tanter, and M. Fink, "Revisiting iterative time reversal processing: Application to detection of multiple targets," *J. Acoust. Soc. Amer.*, vol. 115, no. 2, pp. 776–784, 2004.
[23] Y. Ying-Zi, M. Li, and G. Sheng-Ming, "Adaptive and optimal detection of elastic object scattering with single-channel monostatic iterative time reversal," *Chin. Phys. B*, vol. 20, no. 5, p. 054301, 2011.
[24] G. Micolau, M. Saillard, and P. Borderies, "DORT method as applied to ultrawideband signals for detection of buried objects," *IEEE Trans. Geosci. Remote Sens.*, vol. 41, no. 8, pp. 1813–1820, Aug. 2003.
[25] C. E. Baum, "On the singularity expansion method for the solution of electromagnetic interaction problems," Kirtland AFB USAF, Albuquerque, NM, USA, Interact. Notes #88, Dec. 1971.

[26] A. J. Devaney, E. A. Marengo, and F. K. Gruber, "Time-reversal-based imaging and inverse scattering of multiply scattering point targets," *J. Acoust. Soc. Amer.*, vol. 118, no. 5, pp. 3129–3138, 2005. [Online]. Available: http://scitation.aip.org/content/asa/journal/jasa/118/5/10.1121/1.2042987
[27] F. K. Gruber, E. A. Marengo, and A. J. Devaney, "Time-reversal imaging with multiple signal classification considering multiple scattering between the targets," *J. Acoust. Soc. Amer.*, vol. 115, no. 6, pp. 3042–3047, 2004. [Online]. Available: http://scitation.aip.org/content/asa/journal/jasa/115/6/10.1121/1.1738451
[28] A. J. Devaney, *Mathematical Foundations of Imaging, Tomography and Wavefield Inversion*. Cambridge, U.K.: Cambridge Univ. Press, 2012.
[29] A. Nachbin, J.-P. Fouque, and J. Garnier, "Time reversal for dispersive waves in random media," *SIAM J. Appl. Math.*, vol. 64, no. 5, pp. 1810–1838, 2004.
[30] I. Núñez and C. Negreira, "Efficiency parameters in time reversal acoustics: Applications to dispersive media and multimode wave propagation," *J. Acoust. Soc. Amer.*, vol. 117, no. 3, pp. 1202–1209, 2005.
[31] L. L. Foldy, "The multiple scattering of waves. I. General theory of isotropic scattering by randomly distributed scatterers," *Phys. Rev.*, vol. 67, no. 3, pp. 107–119, Feb. 1945.
[32] M. Cheney and B. Borden, *Fundamentals of Radar Imaging* (CBMS-NSF Regional Conference Series in Applied Mathematics). Philadelphia, PA, USA: SIAM, 2009. [Online]. Available: http://books.google.com/books?id=E7M7HQGB0EwC
[33] C. Prada, S. Manneville, D. Spoliansky, and M. Fink, "Decomposition of the time reversal operator: Detection and selective focusing on two scatterers," *J. Acoust. Soc. Amer.*, vol. 99, no. 4, pp. 2067–2076, 1996. [Online]. Available: http://scitation.aip.org/content/asa/journal/jasa/99/4/10.1121/1.415393
[34] J. Kim, "Time reversal operation for distributed systems in stationary and dynamic environment," Ph.D. dissertation, Dept. Math., Rensselaer Polytech. Inst., Troy, NY, USA, Dec. 2015.
[35] C. E. Baum, "Toward an engineering theory of electromagnetic scattering: The singularity and eigenmode expansion methods," in *Electromagnetic Scattering*, P. L. E. Uslenghi, Ed. San Diego, CA, USA: Academic, 1978, ch. 13, pp. 571–651.
[36] P. D. Lax, *Functional Analysis*. New York, NY, USA: Wiley, 2002.
[37] A. G. Ramm, "Mathematical foundations of singularity and eigenmode expansion methods (SEM and EEM)," *J. Math. Anal. Appl.*, vol. 86, no. 2, pp. 562–591, 1982.
[38] C. E. Baum, E. J. Rothwell, Y. F. Chen, and D. P. Nyquist, "The singularity expansion method and its application to target identification," *Proc. IEEE*, vol. 79, no. 10, pp. 1481–1492, Oct. 1991.
[39] T. K. Sarkar, S. Park, J. Koh, and S. M. Rao, "Application of the matrix pencil method for estimating the SEM (singularity expansion method) poles of source-free transient responses from multiple look directions," *IEEE Trans. Antennas Propag.*, vol. 48, no. 4, pp. 612–618, Apr. 2000.
[40] T. K. Sarkar and O. Pereira, "Using the matrix pencil method to estimate the parameters of a sum of complex exponentials," *IEEE Antennas Propag. Mag.*, vol. 37, no. 1, pp. 48–55, Feb. 1995.
[41] T. Lobos and J. Rezmer, "Spectral estimation of distorted signals using Prony method," *Spectrum*, vol. 6, p. 7, 2003.
[42] M. Hurst and R. Mittra, "Scattering center analysis via Prony's method," *IEEE Trans. Antennas Propag.*, vol. 35, no. 8, pp. 986–988, Aug. 1987.
[43] S. K. Hong, W. S. Wall, T. D. Andreadis, and W. A. Davis. (Apr. 2012). "Practical implications of pole series convergence and the early-time in transient backscatter," Naval Res. Lab., Washington, DC, USA, Tech. Rep. NRL/MR/5740-12-9411. [Online]. Available: http://oai.dtic.mil/oai/oai?verb=getRecord&metadataPrefix=html&identifier=ADA559950
[44] C. Dolph and S. Cho, "On the relationship between the singularity expansion method and the mathematical theory of scattering," *IEEE Trans. Antennas Propag.*, vol. 28, no. 6, pp. 888–897, Nov. 1980.
[45] L. Marin, "Natural-mode representation of transient scattered fields," *IEEE Trans. Antennas Propag.*, vol. AP-21, no. 6, pp. 809–818, Nov. 1973.
[46] M. Hardt and E. Price, "The noisy power method: A meta algorithm with applications," in *Proc. Adv. Neural Inf. Process. Syst.*, 2014, pp. 2861–2869.
[47] L. N. Trefethen and D. Bau, III, *Numerical Linear Algebra*. Philadelphia, PA, USA: SIAM, 1997.

Jerry Kim received the B.S. degree in mathematics from the United States Naval Academy, Annapolis, MD, USA, in 2000, the M.S. degree in physics from the Naval Postgraduate School, Monterey, CA, USA, in 2007, and the M.S. and Ph.D. degrees in mathematics from the Rensselaer Polytechnic Institute, Troy, NY, USA, in 2012 and 2015, respectively.

He served as First Lieutenant on the USS SIMPSON FFG-56 from 2000 to 2003. From 2005 to 2007, he served as Combat Systems Officer on the USS ROBIN MHC-54. He was redesignated as an Engineering Duty Officer in 2004. He then served as Ship Superintendent for the Japan Regional Maintenance Center from 2007 to 2008, where he was responsible for the dry docking and maintenance. He served as the Deputy Shore Branch Head/Project Controller for SPAWAR Systems Facilities Pacific Yokosuka, Japan, from 2008 to 2010, interfacing with the U.S. Seventh Fleet, program office, and the warfare center for the planning and execution of naval programs. He was with the Radar Division, U.S. Naval Research Laboratory, Washington, DC, USA, from 2013 to 2014, and the Tactical Electronic Warfare Division from 2014 to 2016 as a Research Intern.

Margaret Cheney received the B.A. degree in mathematics and physics from Oberlin College, Oberlin, OH, USA, in 1976, the Ph.D. degree in mathematics from Indiana University, Bloomington, IN, USA, in 1982, and the Honorary Doctor of Science degree from Oberlin College in 2011.

She held a post-doctoral position with Stanford University, Stanford, CA, USA, from 1982 to 1984. She was an Assistant Professor with Duke University, Durham, NC, USA, from 1986 to 1988, and an Associate Professor from, 1988 to 1993 and a Professor from 1993 to 2012 with the Rensselaer Polytechnic Institute, Troy, NY, USA. Since 2012, she has been the Albert C. Yates Endowment Professor of Mathematics with Colorado State University, Fort Collins, CO, USA, where she also holds an appointment the Department of Electrical and Computer Engineering. the Department of Electrical and Computer Engineering. She held visiting appointments with the Los Alamos Scientific Laboratory, Los Alamos, NM, USA, from 1976 to 1980, the Ames Laboratory, Ames, IA, USA, from 1985 to 1987, the Naval Air Warfare Center Weapons Division, NAS China Lake, CA, USA, in 2002, the Air Force Research Laboratory from 2007 to 2008, the U.S. Naval Research Laboratory, Washington, DC, USA, in 2012, and Sandia National Laboratories, Albuquerque, NM, USA, in 2016. Most of her work has been on the inverse problems that arise in acoustics and electromagnetics. Since 2001, she has been working on radar imaging. She has published more than 70 refereed articles in international journals, together with a similar number of conference proceedings papers and reports, and has given about 200 invited lectures all over the U.S. and Europe. She holds four patents.

Dr. Cheney is a Fellow of the Institute of Physics and the Society for Industrial and Applied Mathematic (SIAM). She has received several awards, including the Office of Naval Research Young Investigator Award in 1986, a National Science Foundation Faculty Award for Women in Science and Engineering in 1990, and the Lise Meitner Visiting Professorship at the Lund Institute of Technology, Lund, Sweden, in 2000. She was a member of the Rensselaer Impedance Imaging Team that received the 1993 Computer World Smithsonian Award in the Medicine category. She served three terms on the SIAM board of Trustees, and for the last 20 years has served on various SIAM committees. She has served on the Editorial Boards of five journals.

Eric Mokole (F'11) received the B.S. degree in applied mathematics from New York University, New York, NY, USA, in 1971, the M.S. degree in mathematics from Northern Illinois University, DeKalb, IL, USA, in 1973, the M.S. degrees in physics and applied mathematics in 1976 and 1978, respectively, and the Ph.D. degree in mathematics in 1982 from the Georgia Institute of Technology, Atlanta, GA, USA.

He retired in 2014 after 32 years of experience in conducting and leading radar-related research and development and system analyses for existing and proposed U.S. Navy radar programs of record on spaceborne, airborne, shipboard, expeditionary-based, and ultrawideband platforms. These efforts involved: radar waveform diversity and design; radar spectrum theory and engineering; system simulation/modeling; data analysis; information extraction; non-Gaussian detection theory; electronic-warfare and electronic-protection modeling; RF propagation aboard naval ships; tropospheric/ionospheric propagation; pulsed propagation for dispersive media; layered-media propagation; RF scattering from the sea, atmosphere, land, and human-made structures; sensing through the earth and man-made structures; and antenna theory and development. From 1983 to 1986, he held a position in the Electronic Warfare Division, Naval Intelligence Support Center (now the Office of Naval Intelligence), Washington, DC, USA. From 1986 to 2014, he was employed in various roles by the Radar Division, U.S. Naval Research Laboratory in Washington D.C. From 2001 to 2005, he was the Head of the Surveillance Technology Branch. After a period as an Acting Superintendent of Radar from 2005 to 2008, he resumed Branch-Head duties until his retirement in 2014. Currently , he is an Independent Consultant. He has over 85 conference/journal articles, book chapters, and reports and is a Co-Editor/Co-Author of five books (Ultra-Wideband, Short-Pulse Electromagnetics 6,7,10; Physics of Multiantenna Systems and Broadband Processing; Principles of Waveform Diversity and Design). He has presented over 150 talks and tutorials.

Dr. Mokole is the Chair of the AP-S Standing Committee on New Technology Directions, the Co-Chair of the AP-S Committee on the Special Interest Group on Humanitarian Technology, a member of the AP-S Standards Committee, the Chair of the AP-S RCS Measurements Standard Revision (Std 1502), a member of the AP-S Strategic Planning Committee, and a member of the AP-S Member and Geographic Activities Committee. His other professional activities include: member of the IEEE AP-S, AES-S, EMCS, GRS-S, and MTT-S; member of the AES-S Radar Systems Panel since 2006 and its Conference, Waveform Diversity, and Radar Standards Committees; Government Liaison to USNC-URSI from 2009 to 2014, a member of Commissions A/B/C/E, and Secretary and Vice Chair of C; U.S. Member from 2006 to 2014, Vice Chair from 2009 to 2011, and Chair from 2011 to 2014 of NATO's Sensors and Electronics Technology Panel; U.S. Navy Lead for the MSS Tri-Service Radar Symposia from 2005 to 2014, Committee Member of the MSS National Symposia from 2007 to 2014 and the MSS Executive Committee, and an MSS Fellow; Panel Member and Subject Matter Expert of the U.S. Office of Secretary of Defence's Radar Spectrum and Technology Working Group from 2004 to 2005; Founding Member of the Tri-Service Waveform Diversity Working Group since 2002; and AMEREM/EUROEM High-Power Electromagnetics Committee since 2002. He has chaired and served on the organizing committees of numerous conferences.